

Nuclear and neutron matter equations of state from high-quality potentials up to fifth order of the chiral expansion

F. Sammarruca,¹ L. E. Marcucci,^{2,3} L. Coraggio,⁴ J. W. Holt,⁵ N. Itaco,^{4,6} and R. Machleidt¹

¹*Department of Physics, University of Idaho, Moscow, ID 83844, USA*

²*Dipartimento di Fisica “Enrico Fermi”, Università di Pisa, Largo Bruno Pontecorvo 3 - I-56127 Pisa, Italy*

³*Istituto Nazionale di Fisica Nucleare, Sezione di Pisa,*

Largo Bruno Pontecorvo 3 - I-56127 Pisa, Italy

⁴*Istituto Nazionale di Fisica Nucleare, Sezione di Napoli*

Complesso Universitario di Monte S. Angelo, Via Cintia - I-80126 Napoli, Italy

⁵*Cyclotron Institute and Department of Physics and Astronomy,
Texas A & M University, College Station, TX 77843 USA*

⁶*Dipartimento di Matematica e Fisica, Università della Campania “Luigi Vanvitelli”,
Viale Lincoln 5, I-81100, Caserta, Italy*

We present predictions for the equation of state of symmetric nuclear and pure neutron matter based on recent high-quality nucleon-nucleon potentials from leading order to fifth order in the chiral expansion. We include as well the next-to-next-to-leading order (N²LO) chiral three-nucleon force whose low-energy constants c_D and c_E are fitted to the binding energies of ³H and ³He as well as the β -decay lifetime of ³H. The ground state energy per particle is computed in the particle-particle ladder approximation up to a few times saturation density. Due to the soft character of the interactions, uncertainties due to the convergence in many-body perturbation theory are small. We find that nuclear matter saturation is reproduced quantitatively at N³LO and N⁴LO, and therefore we encourage the application of these interactions in finite nuclei, where the description of ground-state energies and charge radii of medium-mass nuclei may be improved.

I. INTRODUCTION

The properties of neutron-rich matter are important for addressing a number of open questions in nuclear physics and nuclear astrophysics, including the location of neutron drip lines, the thickness of neutron skins, and the structure of neutron stars. These questions have in common a strong sensitivity to the nuclear equation of state (EoS), namely the energy per particle as a function of density and composition (set by the isospin asymmetry $\delta_{np} = (\rho_n - \rho_p)/(\rho_n + \rho_p)$, where ρ_n and ρ_p are the neutron and proton number densities, respectively). The symmetry energy, which is defined as the difference in the energy per particle of pure neutron matter and symmetric nuclear matter at a given density, determines to a good approximation also the energy per particle of homogeneous nuclear matter with arbitrary isospin asymmetry. The symmetry energy and its density dependence are therefore a key focus of contemporary theoretical and experimental investigations, and much effort has been devoted to finding correlations between nuclear observables and this property of infinite matter.

Constructing the EoS microscopically from state-of-the-art few-body interactions gives fundamental insight into effective nuclear forces in the medium. High-precision meson-theoretic interactions [1–3] are still frequently employed in contemporary calculations of nuclear matter, structure and reactions. However, in this framework three-nucleon forces (3NFs), or more generally A -nucleon forces with $A > 2$, have only a loose connection with the associated two-nucleon force (2NF) [4], and there exists no clear scheme to quantify and control the theoretical uncertainties. Chiral effective field the-

ory (EFT) [5–7], on the other hand, provides a more systematic approach to construct nuclear many-body forces, which emerge on an equal footing [8] with two-body forces, and to assess theoretical uncertainties through a systematic expansion controlled by the “power counting” [9]. Furthermore, chiral EFT maintains consistency with the symmetries and symmetry breaking pattern of the underlying fundamental theory of strong interactions, quantum chromodynamics (QCD).

For the reasons described above, chiral EFT has evolved into the authoritative approach for developing nuclear forces, and modern applications have focused on few-nucleon reactions [10–15], the structure of light- and medium-mass nuclei [16–30, 33, 41], infinite matter at zero temperature [7, 31, 32, 34–41] and finite temperature [42, 43], and nuclear dynamics and response functions [44–50]. Although satisfactory predictions have been obtained in many cases, specific problems persist. These include the description of bulk properties of medium-mass nuclei, which typically exhibit charge radii that are too small [51] and binding energies that are highly sensitive to the choice of nuclear force and often turn out to be too large [52]. This has led some groups to fit the low-energy constants that parametrize unresolved short-distance physics in chiral nuclear forces directly to the properties of medium-mass nuclei [53] and, indeed, better predictions for other isotopes are then obtained. However, one would prefer a genuine microscopic approach in which the 2NF is fixed by two-nucleon data and the 3NF by three-nucleon data, with no further fine tuning. Applications to systems with $A > 3$ would then be true predictions, though possibly with large uncertainties.

Two recent studies [29, 30] provide indications for how the overbinding problem may be overcome. In these studies, a rather soft nucleon-nucleon (NN) potential (due to renormalization group evolution) together with 3NFs refitted to the ${}^3\text{H}$ binding energy and the ${}^4\text{He}$ charge radius were used to calculate the ground-state properties of closed shell nuclei ranging from ${}^4\text{He}$ to the light Tin isotopes [29, 30]. The ground-state energies were reproduced accurately, while the radii came out slightly too small, but not dramatically different from experiment. These features can be linked to the good nuclear matter saturation properties of the employed 2NF + 3NF combination [32]. In the above example, the 2NF was soft and alone would lead to substantial overbinding in nuclear matter, but the addition of a repulsive 3NF contribution leads to a much better description of the nuclear matter saturation point [32]. On a historical note, the first quantitative explanation for nuclear matter saturation was achieved in this way within the framework of Dirac-Brueckner-Hartree-Fock theory [54–58]. Alternatively, one may start from a relatively repulsive 2NF and then add an attractive, density-dependent 3NF contribution, such as the combination of the Argonne v_{18} (AV18) 2NF [3] plus the Urbana IX 3NF [59]. However, the nuclear matter saturation energy and density cannot be simultaneously reproduced by this combination [60] and medium-mass nuclei are severely underbound [61]. Similar problems occur when the AV18 2NF is combined with the Illinois-7 3NF [61, 62].

In Ref. [63], high-quality soft chiral NN potentials from leading order to fifth order in the chiral expansion were constructed. These interactions are more consistent than those constructed earlier [5, 64, 65], in the sense that the same power counting scheme and cutoff procedures are used at all orders. For these potentials, the very accurate πN low-energy constants (LECs) determined in the Roy-Steiner analysis of Ref. [66] are applied. The uncertainties associated with these LECs are so small that variations within the errors have negligible impact on the construction of the potentials. That the potentials are soft and rather perturbative has been demonstrated in the investigations of Refs. [67, 68]. In the present work, we extend a subset of the chiral nuclear forces in Ref. [63] to include the consistent $N^2\text{LO}$ three-body force with LECs fitted to the binding energies of $A = 3$ nuclei and the triton β -decay lifetime. We then present predictions for the EoS of symmetric nuclear matter (SNM) and pure neutron matter (PNM) based on this family of chiral potentials. We explore the resulting saturation properties, the convergence pattern in the chiral expansion, the impact of the 3NFs at each order, individual contributions of the 3NF, regulator dependence, and the behavior of these potentials with respect to a perturbative expansion of the ground state energy per nucleon.

The manuscript is organized as follows: in Secs. II and III we briefly summarize the main features of the 2NFs and 3NFs employed in this work. The reader is referred to Ref. [63] for a complete and detailed descrip-

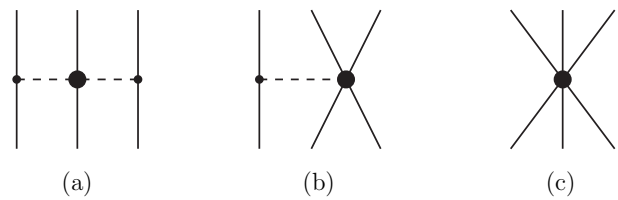


FIG. 1: The 3NF at $N^2\text{LO}$ with (a) the 2PE, (b) the 1PE, and (c) the contact diagrams.

tion of the 2NF. In Sec. IV we present our results for SNM and PNM. Finally, our conclusions are summarized in Sec. V.

II. THE TWO-NUCLEON FORCES

The NN potentials employed in this work span five orders in the chiral EFT expansion, from leading order (LO) to fifth order ($N^4\text{LO}$). The same power counting scheme and regularization procedures are applied through all orders, making this set of interactions more consistent than previous ones. Another novel and important aspect in the construction of these new potentials is the fact that the long-range part of the interaction is fixed by the πN LECs as determined in the recent and very accurate analysis of Ref. [66]. In fact, for all practical purposes, errors in the πN LECs are no longer an issue with regard to uncertainty quantification. Furthermore, at the fifth (and highest) order, the NN data below pion production threshold are reproduced with excellent precision ($\chi^2/\text{datum} = 1.15$).

Iteration of the potential in the Lippmann-Schwinger equation requires cutting off high-momentum components, consistent with the fact that chiral perturbation theory amounts to building a low-momentum expansion. This is accomplished through the application of a regulator function for which the non-local form is chosen:

$$f(p', p) = \exp[-(p'/\Lambda)^{2n} - (p/\Lambda)^{2n}], \quad (1)$$

where $p' \equiv |\vec{p}'|$ and $p \equiv |\vec{p}|$ denote the final and initial nucleon momenta in the center-of-mass system, respectively. For the present applications in nuclear and neutron matter, we will limit ourselves to values of the cutoff parameter Λ smaller than or equal to 500 MeV, as those have been associated with the onset of favorable perturbative properties. The soft nature of the potentials has been confirmed by the Weinberg eigenvalue analysis of Ref. [67] and in the context of the perturbative calculations of infinite matter of Ref. [68].

III. THE THREE-NUCLEON FORCES

Three-nucleon forces make their first appearance at the third order of the chiral expansion ($N^2\text{LO}$). At this order, the 3NF consists of three contributions [10]: the

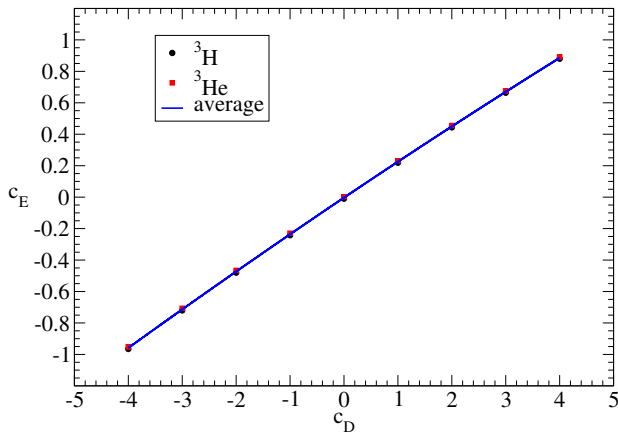


FIG. 2: Trajectory of c_D and c_E obtained by fitting to the ${}^3\text{H}$ or ${}^3\text{He}$ binding energies using the N^4LO NN potential and the N^2LO 3NF with $\Lambda = 450$ MeV. The average trajectory is also shown.

long-range two-pion-exchange (2PE) term, the medium-range one-pion exchange (1PE) diagram, and a short-range contact term. The corresponding diagrams are shown in Fig. 1. We apply these 3NFs by way of the density-dependent effective two-nucleon interactions derived in Refs. [69, 70]. They are expressed in terms of the well-known non-relativistic two-body nuclear force operators and can be conveniently incorporated in the usual NN partial wave formalism and the particle-particle ladder approximation for computing the EoS. The effective density-dependent two-nucleon interactions consist of six one-loop topologies. Three of them are generated from the 2PE graph of the chiral 3NF, Fig. 1(a), and depend on the LECs $c_{1,3,4}$, which are already present in the 2PE part of the NN interaction. Two one-loop diagrams are generated from the 1PE diagram, Fig. 1(b), and depend on the low-energy constant c_D . Finally, there is the one-loop diagram that involves the 3NF contact diagram, Fig. 1(c), with LEC c_E . Note that, in pure neutron matter, the contributions proportional to the LECs c_4 , c_D , and c_E vanish [31]. In recent nuclear matter calculations [39, 68], progress has been made toward including N^3LO three-body interactions in the two-body normal-ordering approximation as well as including the residual three-body normal-ordered force.

We fix the LECs c_D and c_E within the three-nucleon sector. Specifically, we constrain them to reproduce the $A = 3$ binding energies and the Gamow-Teller (GT) matrix element of tritium β -decay, following a well established procedure [71–73]. A few comments are here in order. (i) The regulator function used in the derivation of the 3NF is that of Ref. [74], i.e.

$$f(q) = \exp[(-q/\Lambda)^4], \quad (2)$$

where $q = |\vec{p}' - \vec{p}|$ is the momentum transfer. With this choice, the 3NF is local in coordinate space, making the construction of the $A = 3$ wave functions less involved [75]. (ii) The relation which in Refs. [72, 73]

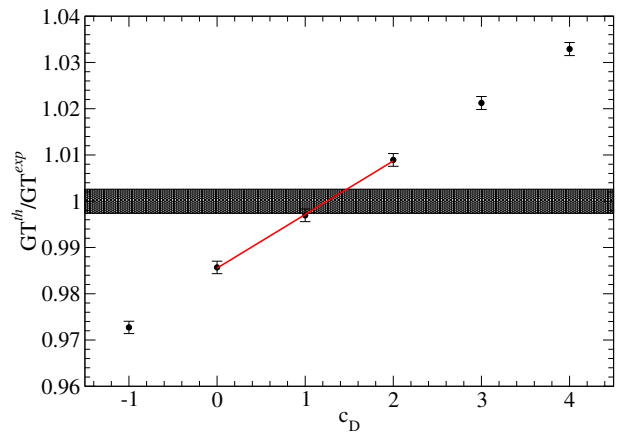


FIG. 3: Ratio $\text{GT}^{th}/\text{GT}^{exp}$ as a function of c_D using the N^4LO NN potential and the N^2LO 3NF with $\Lambda = 450$ MeV. The circles are the calculated values, while the solid (red) line is a linear fit in the region where the experimental band is crossed.

was used to relate the LEC c_D with d_R , the LEC entering the axial current at N^2LO , has been recently revisited [73, 76]. While in Refs. [72, 73] it was

$$d_R = \frac{m}{g_A \Lambda_\chi} c_D + \frac{m}{3} (c_3 + 2c_4) + \frac{1}{6}, \quad (3)$$

m being the nucleon mass, g_A the single-nucleon axial coupling constant (here $g_A = 1.2723$ [77]), Λ_χ the chiral-symmetry-breaking scale (here $\Lambda_\chi = 1$ GeV), in Ref. [76] it was shown that the correct relation is

$$d_R = -\frac{m}{4g_A \Lambda_\chi} c_D + \frac{m}{3} (c_3 + 2c_4) + \frac{1}{6}. \quad (4)$$

This has been confirmed also in Ref. [78]. We note that the muon capture rates calculated in Ref. [73] have remained unchanged. This is not surprising, since the LECs c_D and c_E originally used in the axial current of the muon capture (as well as proton weak capture of Ref. [79]) lead to the same enhancement as in Ref. [73] needed to reproduce the tritium GT matrix element.

For the sake of completeness, we recall the various steps for the adopted fitting procedure, which are: (i) determination of a $c_D - c_E$ trajectory, obtained by reproducing the ${}^3\text{H}$ and ${}^3\text{He}$ binding energies. Typically, the ${}^3\text{H}$ and ${}^3\text{He}$ trajectories are indistinguishable, and the average can be safely used, leading to the $A = 3$ binding energies within ~ 10 keV of the experimental ones. (ii) For each set of $c_D - c_E$ values, we have calculated the GT matrix element of tritium β -decay and fitted to its experimental value, taken as in Ref. [77] to be 0.9511 ± 0.0013 . We have then found a range of c_D values, for which the theoretical and experimental GT values, GT^{th} and GT^{exp} respectively, coincide (note that we have conservatively doubled the experimental error on GT^{exp}). The corresponding values for c_E are obtained from the $c_D - c_E$ trajectory mentioned above. In Table I we list the central values of the LECs c_D and c_E

TABLE I: Values of the LECs $c_{1,3,4}$, c_D , and c_E for different orders in the chiral EFT expansion and different values of the momentum-space cutoff Λ . The LECs $c_{1,3,4}$ are given in units of GeV^{-1} , while c_D and c_E are dimensionless. The numbers in parentheses indicate the error arising from the fitting procedure. In addition, we also show the value for the exponent n that appears in the regulator function of Eq. (1).

	Λ (MeV)	n	c_1	c_3	c_4	c_D	c_E
N ² LO	450	2	-0.74	-3.61	2.44	0.935(0.215)	0.12(0.04)
	500	2	-0.74	-3.61	2.44	0.495(0.195)	-0.07(0.04)
N ³ LO	450	2	-1.07	-5.32	3.56	0.675(0.205)	0.31(0.05)
	500	2	-1.07	-5.32	3.56	-0.945(0.215)	-0.68(0.04)
N ⁴ LO	450	2	-1.10	-5.54	4.17	1.245(0.225)	0.28(0.05)
	500	2	-1.10	-5.54	4.17	-0.670(0.230)	-0.83(0.03)

TABLE II: Same as Table I, but including the 2PE 3NF at fourth and fifth order, respectively. (The N²LO numbers are the same as in Table I.)

	Λ (MeV)	n	c_1	c_3	c_4	c_D	c_E
N ² LO	450	2	-0.74	-3.61	2.44	0.935(0.215)	0.12(0.04)
	500	2	-0.74	-3.61	2.44	0.495(0.195)	-0.07(0.04)
N ³ LO	450	2	-1.20	-4.43	2.67	0.670(0.210)	0.41(0.05)
	500	2	-1.20	-4.43	2.67	-0.750(0.210)	-0.41(0.04)
N ⁴ LO	450	2	-0.73	-3.38	1.69	0.560(0.220)	0.46(0.05)
	500	2	-0.73	-3.38	1.69	-0.745(0.225)	-0.15(0.04)

used in this work, with the error in parentheses arising from the fitting procedure. Obviously, these values have been obtained using Eq. (4). As we can see by inspection of the table, the allowed range for c_D is quite large, while the corresponding one for c_E is much smaller. Since the c_D contribution to the energy per particle in SNM is very small (see below), we do not include this uncertainty in the present calculations. As an example, we show in Fig. 2 the $c_D - c_E$ trajectory and in Fig. 3 the ratio $\text{GT}^{th}/\text{GT}^{exp}$ as a function of c_D for the N⁴LO NN potential and the N²LO 3NF with $\Lambda = 450$ MeV.

The complete 3NF beyond N²LO is very complex and often neglected in nuclear structure studies, but progress toward the inclusion of the subleading 3NF at N³LO is underway [39, 68, 80, 81]. There is one important component of the 3NF where complete calculations up to N⁴LO are possible: the 2PE 3NF. In Ref. [82] it was shown that the 2PE 3NF has essentially the same analytical structure at N²LO, N³LO, and N⁴LO. Thus, one can add the three orders of 3NF contributions and parametrize the result in terms of effective LECs.

In the N⁴LO rows of Table II we give the effective LECs $c_{1,3,4}$ obtained in Ref. [82]. Concerning the 2PE 3NF at N³LO, Eq. (2.8) of Ref. [83] provides the corrections to the c_i but there is an error in the numerical values given below this equation. While $\delta c_1 = -0.13 \text{ GeV}^{-1}$ is correct, the correct values for δc_3 and δc_4 are $\delta c_3 = -\delta c_4 = 0.89 \text{ GeV}^{-1}$. When these corrections are applied, the values given in the N³LO rows of Table II emerge. By using the c_i of Table II in the mathematical expression of the N²LO 3NF, one can include the 2PE

parts of the 3NF up to N³LO and up to N⁴LO in a simple way. Consequently, the LECs c_D and c_E are fitted again with the same procedure outlined above. Their values are also listed in Table I but of the same order and with the same sign. Among all possible 3NF contributions, the 2PE 3NF is historically the first calculated [84]. The prescriptions given above allow us to incorporate this very important 3NF up to the highest orders considered in this paper.

IV. CALCULATIONS OF THE EQUATION OF STATE

We perform microscopic calculations of nuclear and neutron matter with the interactions described above. We compute the EoS using the nonperturbative particle-particle ladder approximation, which generates the leading-order contributions in the traditional hole-line expansion. In addition we compute the single-particle spectrum for the intermediate-state energies also in the particle-particle ladder approximation, keeping only the real part.

A. Nuclear matter: predictions and discussion

We begin with the study displayed in Fig. 4, where the momentum-space cutoff is fixed at 450 MeV but the chiral order of the two-body force is varied from leading

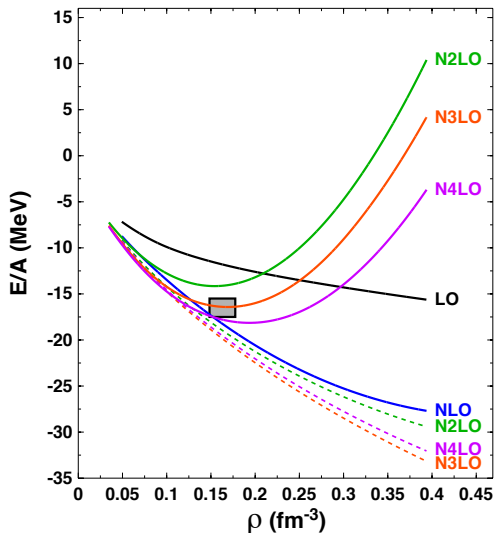


FIG. 4: Ground state energy per particle of SNM as a function of density from the chiral two- and three-body forces with cutoff $\Lambda = 450$ MeV. The three dotted curves show predictions which include only two-body forces. For the 3NF contributions at N²LO and above, the LECs of Table II are used. The shaded box denotes the approximate empirical saturation energy and density.

to fifth order. The 3NFs are chosen with LECs in Table II, which at N³LO and N⁴LO include the 2PE 3NF at fourth and fifth order, respectively. The dashed lines indicate results at N²LO and above with no three-body forces present, while the solid lines include the N²LO three-body force when appropriate. Formally, we observe a good convergence pattern at the two-body level with this family of NN potentials, but naturally we do not expect realistic saturation behavior when soft two-body forces alone are included in the calculation of the EoS. We see that the inclusion of 3NFs is necessary beyond about half nuclear matter saturation density and that for this set of nuclear potentials the total 3NF contribution to the EoS decreases with the chiral order from N²LO to N⁴LO.

We note that the uncertainty band obtained by varying the chiral order from N²LO to N⁴LO while keeping $\Lambda = 450$ MeV fixed encloses the empirical saturation point. The saturation energy varies in the range $-14 \text{ MeV} \lesssim E_0 \lesssim -18 \text{ MeV}$ while the saturation density varies between $0.155 \text{ fm}^{-3} \lesssim \rho_0 \lesssim 0.195 \text{ fm}^{-3}$. We stress that once the two- and three-nucleon forces are fixed by the NN data and the properties of the three-nucleon system, no parameters are finely tuned, rendering the many-body calculation parameter-free. Since the predicted binding energies and charge radii of intermediate-mass nuclei are closely related to the corresponding saturation point in SNM, we see first evidence that the new class of chiral potentials constructed in this work may lead to more reliable predictions in ab initio calculations of finite nuclei. For densities larger than $\rho \gtrsim 0.20 \text{ fm}^{-3}$,

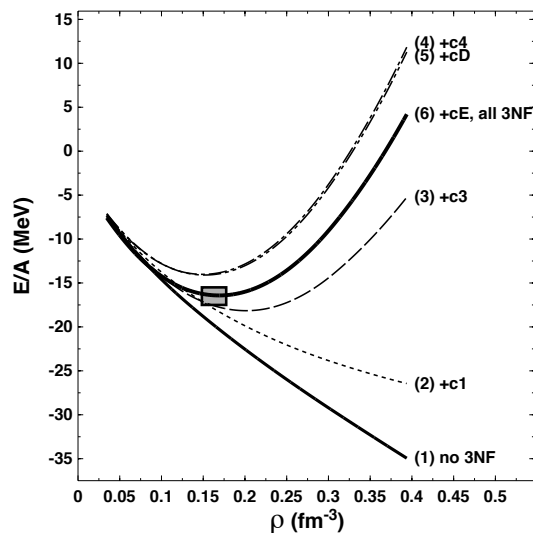


FIG. 5: Ground state energy per particle of SNM as a function of density from the N³LO interaction with a cutoff of 450 MeV. Curves are numbered in ascending order to denote that each has been obtained from the previous one with the addition of the indicated 3NF contribution. Other details as in Fig. 4.

the predictions shown in Fig. 4 display a trend that does not suggest satisfactory convergence, since the three (saturating) solid curves are about equally spaced. This may be due to the incompleteness of the 3NF at orders above N²LO.

Next we present in Fig. 5 the contribution to the SNM EoS from individual 3NF terms proportional to the LECs $c_{1,3,4}$, c_D , and c_E . We have chosen the case of the N³LO NN interaction with a cutoff of 450 MeV together with the 3NF LECs from Table II. We observe that the total contribution from terms proportional to c_3 is very large and instrumental for nuclear saturation. Both the c_1 and c_4 terms generate additional repulsion, while the single contribution from the c_E term is attractive in this parametrization. Only the c_D term is negligible in this case, even though numerically it is of natural size.

In Fig. 6 we show the dependence of the SNM EoS on the choice of momentum-space cutoff Λ in the two- and three-body forces as well as the order in the chiral expansion. In the present work we consider only the two cases $\Lambda = 450, 500$ MeV. The nuclear potentials constructed in [63] with $\Lambda = 550$ MeV were found to have marginal convergence properties in many-body perturbation theory and therefore not considered in the present work. At orders N²LO, N³LO, and N⁴LO, the cutoff dependence appears to be comparable but generically smaller than the truncation errors.

In Fig. 7, we show the impact of choosing at fourth and fifth order in the chiral expansion either the N²LO 3NF coupling strengths shown in Table I (labeled “I” in the figure) or those obtained by including the 2PE 3NF contributions at higher order shown in Table II (labeled “II”

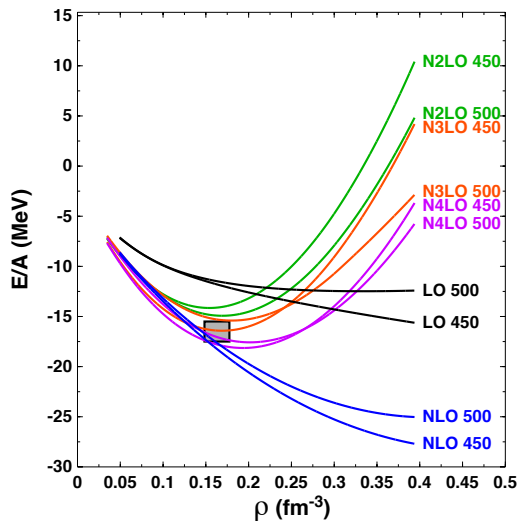


FIG. 6: Ground state energy per particle of SNM as a function of density at the indicated orders and with varying cutoff parameters as denoted. Other details as in Fig. 4.

in the figure). We only show results for potentials with momentum-space cutoff $\Lambda = 450$ MeV, but we expect qualitatively similar results for the $\Lambda = 500$ MeV cutoff potentials due to the identical change in the important c_i low-energy constants. We see that at N^4 LO the impact is rather large and roughly of the same size as variations in the chiral order from N^2 LO to N^4 LO. However, the additional theoretical uncertainty resulting from the choice of LECs entering into the 2PE 3NF would extend only moderately the overall error band inferred from Fig. 6 and only at the largest densities considered.

Finally, we investigate the theoretical uncertainties associated with our many-body method. For this purpose we compare the results obtained within the preceding nonperturbative particle-particle ladder-diagram summation (NPLDS) technique with calculations in many-body perturbation theory (MBPT). This may be especially useful for practitioners who intend to employ MBPT for nuclear structure calculations with the new set of chiral forces. The perturbative expansion of the ground-state energy per particle is performed up to third-order in particle-particle ladder diagrams within the same formalism found in Ref. [36]. In particular, we employ a Hartree-Fock spectrum for the intermediate-state energies appearing in the second- and third-order diagrams. We also calculate the [2|1] Padé approximant of the MBPT expansion (see Refs. [36, 37]). The difference between third-order MBPT in the particle-particle channel, [2|1] Padé approximant, and NPLDS gives an indication of the quality of the perturbative behavior of the new potentials.

First, we consider the SNM EoS in the presence of 2NFs only. In this case, the results of MBPT are almost identical to those obtained using either the [2|1] Padé approximant or the NPLDS, the latter already reported in

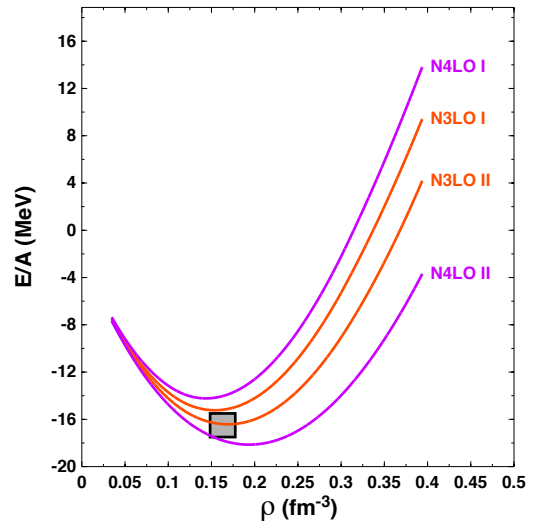


FIG. 7: Energy per particle in SNM as a function of density at N^3 LO and N^4 LO with a cutoff of $\Lambda = 450$ MeV. For the 3NF contributions, the LECs of either Table I or Table II are applied as indicated by labels ‘I’ or ‘II’, respectively. Case ‘II’ is characterized by including the 2PE 3NF up to the given order. The shaded box denotes the approximate empirical saturation energy and density.

Figs. 4 and 6. We find that the above feature is independent of the order of the chiral expansion and the choice of the cutoff. The perturbative nature of the new chiral 2NFs makes therefore them suitable for nuclear structure calculations.

On the other hand, inclusion of the 3NF alters the perturbative behavior of the ground-state energy per nucleon in SNM. The degree of variation in the perturbative behavior depends on the order in the chiral EFT expansion and the choice of the cutoff. In Fig. 8, we show the EoS predictions for the $\Lambda = 450, 500$ MeV chiral potentials with 3NF ‘II’ low-energy constants from N^2 LO to N^4 LO. Results are obtained for three different scenarios: third-order MBPT (particle-particle channel), its [2|1] Padé approximant, and the NPLDS. The differences between the MBPT and NPLDS results are due primarily to the choice of single-particle spectrum in intermediate-states. In the NPLDS the spectrum is more compressed relative to the Hartree-Fock spectrum employed in MBPT, leading to an enhancement of the large attraction appearing at second-order. For the larger cutoff value of $\Lambda = 500$ MeV, the differences between the NPLDS and MBPT are generically larger. We also observe that the discrepancies between the two methods are smaller at N^2 LO and N^4 LO as compared to N^3 LO. For $\Lambda = 450$ MeV, however, the perturbative behavior is quite good across all scenarios considered.

We conclude this section with additional comments on the important issue of SNM saturation. In the recent work of Ref. [29], the aim was to explore the impact of SNM saturation on the properties of closed and open-shell nuclei with $A \leq 78$. In another investiga-

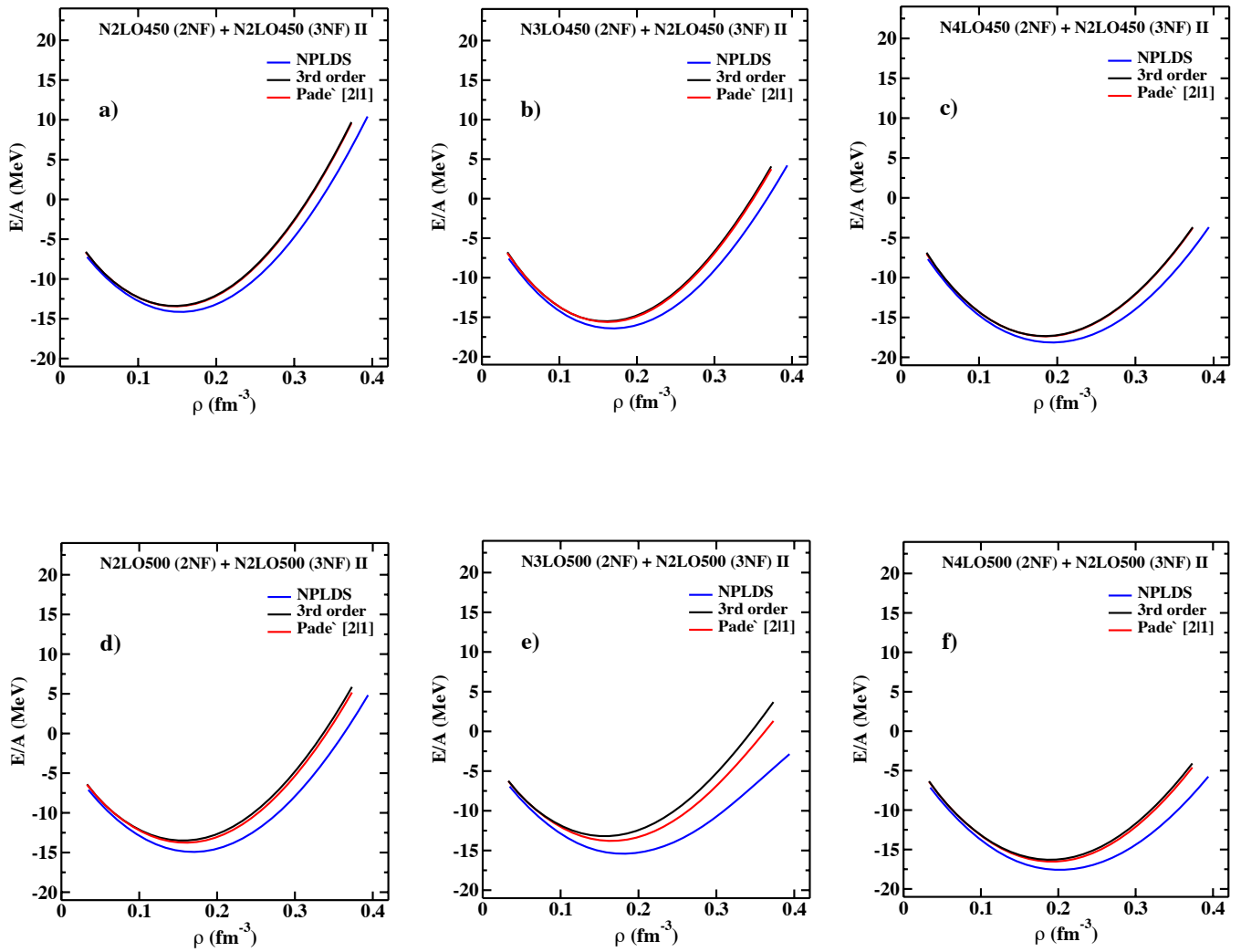


FIG. 8: The SNM EoS from the $\Lambda = 450$ MeV (upper panel) and the $\Lambda = 500$ MeV (lower panel) chiral potentials. Results are calculated in three ways: (i) NPLDS, (ii) MBPT including up to third-order particle-particle diagrams, and (iii) the [2|1] Padé approximant. The 3NF LECs from Table II are used in all cases.

tion [30], in which the same forces were applied, the structure of the light Sn isotopes were studied, reproducing both the binding energy and the small splitting between the lowest $J^\pi = 7/2^+$ and $5/2^+$ states of ^{100}Sn . In those studies, the N^3LO potential ($\Lambda = 500$ MeV) of Ref. [64] was taken as the starting point and then evolved through similarity renormalization group (SRG) transformation into low-resolution interactions (i.e., soft interactions). These SRG-evolved NN interactions were then combined with the leading chiral 3NF (with c_D and c_E coupling strengths refitted to the ^3H binding energy and ^4He charge radius) to obtain various Hamiltonians with different cutoff combinations [32]. Ideally, it would be preferable to construct from the outset perturbative two-body forces that do not require additional RG evolution with associated uncontrolled induced many-body forces. From the results of this section, we suggest that the new set of chiral nuclear forces developed in the

present work may produce equally favorable results as those of Refs. [29, 30, 32], and we encourage studies of nuclear systematics based upon these potentials.

B. Neutron matter: predictions and discussion

We next consider the ground state energy of pure neutron matter as a function of density, employing the same set of chiral potentials and many-body methods discussed previously in the case of symmetric nuclear matter. The EoS for both SNM and PNM are crucial to determine the density-dependent nuclear symmetry energy and to better understand the properties of neutron-rich nuclei and neutron stars.

In Fig. 9 we show the energy per particle of PNM as a function of density starting from chiral two- and three-body forces with the same value of the momentum-space

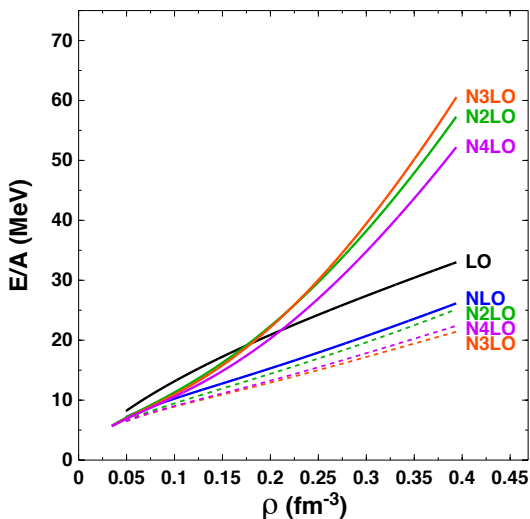


FIG. 9: Ground state energy per particle of PNM as a function of density at the indicated orders in the chiral expansion. The three dotted curves show predictions including only the 2NF. The cutoff parameter is fixed at $\Lambda = 450$ MeV and the 3NF LECs from Table II are used.

cutoff $\Lambda = 450$ MeV but at different orders in the chiral expansion. As in the case of symmetric nuclear matter, we observe good convergence at the level of 2NF alone. When 3NFs are included, we find somewhat smaller truncation errors compared to the case of SNM. This may be due in part to the absence of large, central isospin-0 partial waves in PNM, which appear to be more sensitive to differences among interactions. As shown in Fig. 10, the low-energy constant c_3 is responsible for essentially all of the additional repulsion generated from the two-pion-exchange three-body force. Clearly, the 3NF plays an outstanding role in very neutron-rich systems at and beyond nuclear saturation density, where its contribution to the EoS grows more strongly with the density than the 2NF contributions.

We show in Fig. 11 the energy per particle of pure neutron matter as a function of density when varying both the order in the chiral expansion and the momentum-space cutoff $\Lambda = 450, 500$ MeV. We see that in comparison to the analogous study in symmetric nuclear matter, the pure neutron matter results display a much weaker cutoff dependence, which may again be due to the absence of strong isospin-0 partial waves. Interestingly, even in the case of the relatively large density $\rho = 0.4 \text{ fm}^{-3}$ corresponding to a Fermi momentum of $k_F = 450$ MeV that lies at the effective breakdown scale of the expansion, there is relatively little cutoff dependence.

The impact of including the 2PE 3NF at fourth and fifth order, compared to including only the third-order contributions, through the adoption of the LECs given in Table II is demonstrated in Fig. 12. As in the case of symmetric nuclear matter, the effect at N⁴LO is much larger than that at N³LO due to the larger change $\Delta c_3 =$

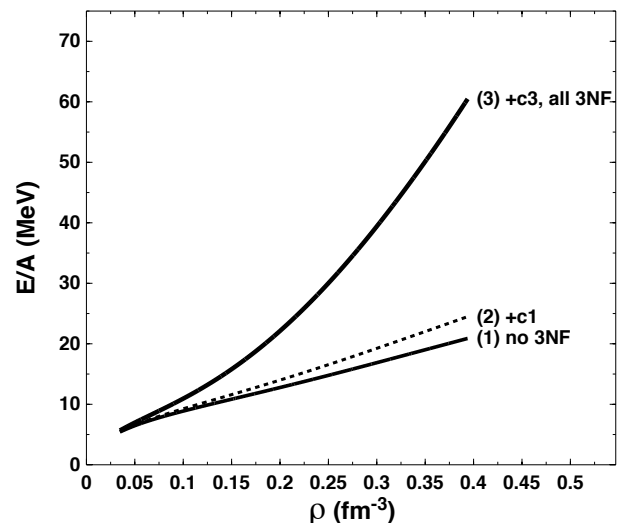


FIG. 10: Ground state energy per particle in PNM as a function of density at N³LO and with a cutoff of 450 MeV. Curves are numbered in ascending order to signify that each has been obtained from the previous one with the addition of the indicated 3NF contribution. Note that the 3NF contributions depending on c_4 , c_D , and c_E vanish in PNM. The LECs of Table II are used.

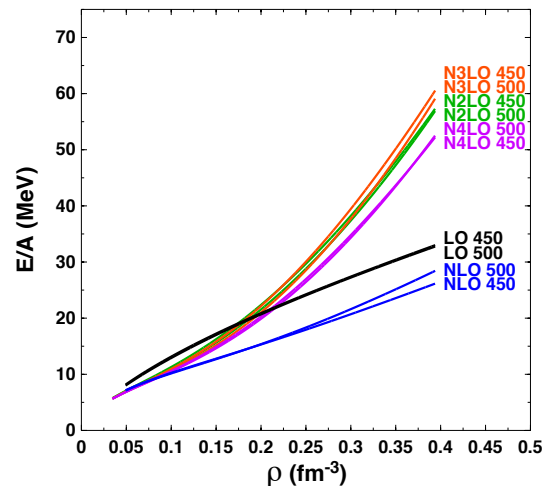


FIG. 11: Ground state energy per particle of PNM as a function of density at the indicated chiral orders and with varying cutoff parameters as denoted. The LECs of Table II are used.

1.94 GeV^{-1} vs. $\Delta c_3 = 0.89 \text{ GeV}^{-1}$, respectively, in the c_3 low-energy constant at these two orders in the chiral expansion. Moreover, the choice of LECs entering into the 2PE 3NF contributions again results in a moderate systematic increase in the pure neutron matter energy per particle at the highest densities considered. It will be interesting to explore the influence of such higher-order 3NF contributions on predictions of neutron star properties. This investigation is in progress.

Regarding the perturbative properties of the PNM EoS, we have found that the results obtained using

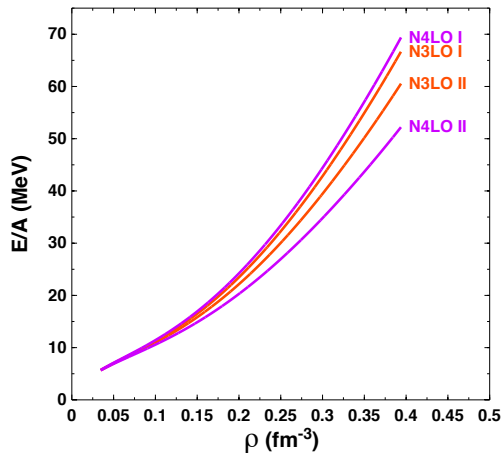


FIG. 12: Ground state energy per particle of PNM as a function of density at $N^3\text{LO}$ and $N^4\text{LO}$ with a cutoff of 450 MeV. Similar to Fig. 7, for the 3NF contributions the LECs of either Table I or Table II are applied as indicated by labels ‘I’ or ‘II’, respectively.

MBPT up to third order in the particle-particle channel, with and without inclusion of 3NF, are consistent with those shown in Figs. 9 – 12. The good perturbative behavior is independent of the choice of cutoff Λ as well as the chiral order at which the nuclear potentials have been derived. We also find the results to be consistent with those obtained in Ref. [36].

V. CONCLUSIONS AND OUTLOOK

In the present work we have extended the new class of chiral NN interactions from LO to $N^4\text{LO}$ in Ref. [63] to

include the complete set of three-nucleon forces at $N^2\text{LO}$ in the chiral expansion. The additional LECs c_D and c_E that appear at this order are fitted to the binding energies of $A = 3$ nuclei and the β -decay lifetime of ^3H . We have included as well the two-pion-exchange three-body forces at $N^3\text{LO}$ and $N^4\text{LO}$ in order to probe the effect of missing higher-order many-body contributions. The resulting set of nuclear potentials were then employed in studies of the nuclear and neutron matter EoS [85]. We find quite good nuclear matter saturation properties together with relatively small uncertainties in the PNM EoS even up to relatively large densities. Moreover, the calculation of the EoS within many-body perturbation theory exhibits quite good behavior with cutoff $\Lambda = 450$ MeV and satisfactory behavior with cutoff $\Lambda = 500$ MeV. While complete calculations at $N^3\text{LO}$ and $N^4\text{LO}$ are the ultimate goal, we suggest that the present set of high-quality potentials will be valuable for systematic studies of medium-mass and heavy nuclei as well as studies of neutron star structure.

Acknowledgments

The work of F.S. and R.M. was supported in part by the U.S. Department of Energy, Office of Science, Office of Basic Energy Sciences, under Award Number DE-FG02-03ER41270. The work of J.W.H. was supported by the National Science Foundation under Grant No. PHY1652199 and the NNSA through DOE Cooperative Agreement de-na0003841. Computational resources provided by the INFN-Pisa Computer Center are gratefully acknowledged.

-
- [1] R. Machleidt, Phys. Rev. C **63** 024001 (2001).
 - [2] V. G. J. Stoks, R. A. M. Klomp, C. P. F. Terheggen, and J. J. de Swart, Phys. Rev. C **49**, 2950 (1994).
 - [3] R. B. Wiringa, V. G. J. Stoks, and R. Schiavilla, Phys. Rev. C **51**, 38 (1995).
 - [4] R. Machleidt, Int. J. Mod. Phys. E **26**, 1730005 and 1740018 (2017).
 - [5] R. Machleidt and D.R. Entem, Phys. Rep. **503**, 1 (2011).
 - [6] E. Epelbaum, H.-W. Hammer, and U.-G. Meissner, Rev. Mod. Phys. **81**, 1773 (2009).
 - [7] R. Machleidt and F. Sammarruca, Phys. Scripta **91**, 083007 (2016).
 - [8] S. Weinberg, Phys. Lett. B **295**, 114 (1992).
 - [9] S. Weinberg, Phys. Lett. B **251**, 288 (1990); Nucl. Phys. B **363**, 3 (1991).
 - [10] E. Epelbaum, A. Nogga, W. Glöckle, H. Kamada, U.-G. Meißner, and H. Witala, Phys. Rev. C **66**, 064001 (2002).
 - [11] P. Navratil, R. Roth, and S. Quaglioni, Phys. Rev. C **82**, 034609 (2010).
 - [12] M. Viviani, L. Girlanda, A. Kievsky, and L. E. Marcucci, Phys. Rev. Lett. **111**, 172302 (2013).
 - [13] J. Golak *et al.*, Eur. Phys. J. A **50**, 177 (2014).
 - [14] N. Kalantar-Nayestanaki, E. Epelbaum, J. G. Messchendorp, and A. Nogga, Rept. Prog. Phys. **75**, 016301 (2012).
 - [15] P. Navratil, S. Quaglioni, G. Hupin, C. Romero-Redondo, and A. Calci, Phys. Scripta **91**, 053002 (2016).
 - [16] L. Coraggio, A. Covello, A. Gargano, N. Itaco, T. T. S. Kuo, D. R. Entem, and R. Machleidt, Phys. Rev. C **75**, 024311 (2007).
 - [17] L. Coraggio, A. Covello, A. Gargano, and N. Itaco, Phys. Rev. C **81**, 064303 (2010).
 - [18] L. Coraggio, A. Covello, A. Gargano, N. Itaco, and T. T. S. Kuo, Ann. Phys. **327**, 2125 (2012).
 - [19] H. Hagen, M. Hjorth-Jensen, G. R. Jansen, R. Machleidt, and T. Papenbrock, Phys. Rev. Lett. **108**, 242501 (2012).
 - [20] H. Hagen, M. Hjorth-Jensen, G. R. Jansen, R. Machleidt, and T. Papenbrock, Phys. Rev. Lett. **109**, 032502 (2012).
 - [21] B. R. Barrett, P. Navratil, and J. P. Vary, Prog. Part. Nucl. Phys. **69**, 131 (2013).

- [22] H. Hergert, S. K. Bogner, S. Binder, A. Calci, J. Langhammer, R. Roth, and A. Schwenk, *Phys. Rev. C* **87**, 034307 (2013).
- [23] G. Hagen, T. Papenbrock, M. Hjorth-Jensen, and D. J. Dean, *Rept. Prog. Phys.* **77**, 096302 (2014).
- [24] V. Somà, A. Cipollone, C. Barbieri, P. Navrátil, and T. Duget, *Phys. Rev. C* **89**, 061301(R) (2014).
- [25] K. Hebeler, J. D. Holt, J. Menéndez, and A. Schwenk, *Ann. Rev. Nucl. Part. Sci.* **65**, 457 (2015).
- [26] G. Hagen *et al.*, *Nature Phys.* **12**, 186 (2015).
- [27] J. Carlson, S. Gandolfi, F. Pederiva, S. C. Pieper, R. Schiavilla, K. E. Schmidt, and R. B. Wiringa, *Rev. Mod. Phys.* **87**, 1067 (2015).
- [28] H. Hergert, S. K. Bogner, T. D. Morris, A. Schwenk, and K. Tsukiyama, *Phys. Rep.* **621**, 165 (2016).
- [29] J. Simonis, S. R. Stroberg, K. Hebeler, J. D. Holt, and A. Schwenk, *Phys. Rev. C* **96**, 014303 (2017).
- [30] T. D. Morris, J. Simonis, S. R. Stroberg, C. Stumpf, G. Hagen, J. D. Holt, G. R. Jansen, T. Papenbrock, R. Roth, and A. Schwenk, arXiv:1709.02786 [nucl-th].
- [31] K. Hebeler and A. Schwenk, *Phys. Rev. C* **82**, 014314 (2010).
- [32] K. Hebeler, S. K. Bogner, R. J. Furnstahl, A. Nogga, and A. Schwenk, *Phys. Rev. C* **83**, 031301(R) (2011).
- [33] A. Gezerlis, I. Tews, E. Epelbaum, S. Gandolfi, K. Hebeler, A. Nogga, and A. Schwenk, *Phys. Rev. Lett.* **111**, 032501 (2013).
- [34] G. Baardsen, A. Ekström, G. Hagen and M. Hjorth-Jensen, *Phys. Rev. C* **88**, 054312 (2013).
- [35] G. Hagen, T. Papenbrock, A. Ekström, K. A. Wendt, G. Baardsen, S. Gandolfi, M. Hjorth-Jensen, and C. J. Horowitz, *Phys. Rev. C* **89**, 014319 (2014).
- [36] L. Coraggio, J. W. Holt, N. Itaco, R. Machleidt, and F. Sammarruca, *Phys. Rev. C* **87**, 014322 (2013).
- [37] L. Coraggio, J. W. Holt, N. Itaco, R. Machleidt, L. E. Marcucci, and F. Sammarruca, *Phys. Rev. C* **89**, 044321 (2014).
- [38] F. Sammarruca, L. Coraggio, J. W. Holt, N. Itaco, R. Machleidt, and L. E. Marcucci, *Phys. Rev. C* **91**, 054311 (2015).
- [39] C. Drischler, A. Carbone, K. Hebeler, and A. Schwenk, *Phys. Rev. C* **94**, 054307 (2016).
- [40] I. Tews, S. Gandolfi, A. Gezerlis, and A. Schwenk, *Phys. Rev. C* **93**, 024305 (2016).
- [41] J. W. Holt and N. Kaiser, *Phys. Rev. C* **95**, 034326 (2017).
- [42] C. Wellenhofer, J. W. Holt, N. Kaiser, and W. Weise, *Phys. Rev. C* **89**, 064009 (2014).
- [43] C. Wellenhofer, J. W. Holt, and N. Kaiser, *Phys. Rev. C* **92**, 015801 (2015).
- [44] S. Bacca, K. Hally, C. J. Pethick, and A. Schwenk, *Phys. Rev. C* **80**, 032802 (2009).
- [45] A. Bartl, C. J. Pethick, and A. Schwenk, *Phys. Rev. Lett.* **113** 081101 (2014).
- [46] E. Rrapaj, J. W. Holt, A. Bartl, S. Reddy, and A. Schwenk, *Phys. Rev. C* **91**, 035806 (2015).
- [47] M. Buraczynski and A. Gezerlis, *Phys. Rev. Lett.* **116**, 152501 (2016).
- [48] J. W. Holt, N. Kaiser, and G. A. Miller, *Phys. Rev. C* **93**, 064603 (2016).
- [49] J. Birkhan *et al.*, *Phys. Rev. Lett.* **118**, 252501 (2017).
- [50] J. Rotureau, P. Danielewicz, G. Hagen, F. Nunes, and T. Papenbrock, *Phys. Rev. C* **95**, 024315 (2017).
- [51] V. Lapoux, V. Somà, C. Barbieri, H. Hergert, J. D. Holt, and S. R. Stroberg, *Phys. Rev. Lett.* **117**, 052501 (2016).
- [52] S. Binder, J. Langhammer, A. Calci, and R. Roth, *Phys. Lett. B* **736**, 119 (2014).
- [53] A. Ekström *et al.*, *Phys. Rev. C* **91**, 051301 (2015).
- [54] R. Brockmann and R. Machleidt, *Phys. Lett.* **149B**, 283 (1984); *Phys. Rev. C* **42**, 1965 (1990).
- [55] D. Alonso and F. Sammarruca, *Phys. Rev. C* **67**, 054301 (2003).
- [56] F. Sammarruca, arXiv:0807.0263 [nucl-th].
- [57] F. Sammarruca, B. Chen, L. Coraggio, N. Itaco, and R. Machleidt, *Phys. Rev. C* **86**, 054317 (2012).
- [58] H. Muether, F. Sammarruca, and Z. Ma, *Int. J. Mod. Phys. E* **26**, 173001 (2017).
- [59] B. S. Pudliner, V. R. Pandharipande, J. Carlson, and R. B. Wiringa, *Phys. Rev. Lett.* **74**, 4396 (1995).
- [60] A. Akmal, V. R. Pandharipande, and D. G. Ravenhall, *Phys. Rev. C* **58**, 1804 (1998).
- [61] D. Lonardoni, A. Lovato, S. C. Pieper, and R. B. Wiringa, *Phys. Rev. C* **96**, 024326 (2017).
- [62] S. C. Pieper, *AIP Conference Proceedings* **1011**, 143 (2008).
- [63] D.R. Entem, R. Machleidt, and Y. Nosyk, *Phys. Rev. C* **96**, 024004 (2017).
- [64] D.R. Entem and R. Machleidt, *Phys. Rev. C* **68**, 041001, (2003).
- [65] E. Marji, A. Canul, Q. MacPherson, R. Winzer, Ch. Zoli, D.R. Entem, and R. Machleidt, *Phys. Rev. C* **88**, 054002 (2013).
- [66] M. Hoferichter, J. Ruiz, de Elvira, B. Kubis, and U.-G. Meissner, *Phys. Rev. Lett.* **115**, 192301 (2015); *Phys. Rep.* **625**, 1 (2016).
- [67] J. Hoppe, C. Drischler, R. J. Furnstahl, K. Hebeler, and A. Schwenk, *Phys. Rev. C* **96**, 054002 (2017).
- [68] C. Drischler, K. Hebeler and A. Schwenk, arXiv:1710.08220 [nucl-th].
- [69] J. W. Holt, N. Kaiser, and W. Weise, *Phys. Rev. C* **79**, 054331 (2009).
- [70] J. W. Holt, N. Kaiser, and W. Weise, *Phys. Rev. C* **81**, 024002 (2010).
- [71] A. Gardestig and D. R. Phillips, *Phys. Rev. Lett.* **96**, 232301 (2006).
- [72] D. Gazit, S. Quaglioni, and P. Navrátil, *Phys. Rev. Lett.* **103**, 102502 (2009).
- [73] L. E. Marcucci, A. Kievsky, S. Rosati, R. Schiavilla, and M. Viviani, *Phys. Rev. Lett.* **108**, 052502, (2012); Erratum: accepted for publication in *Phys. Rev. Lett.* (2018).
- [74] P. Navrátil, *Few-Body Syst.* **41**, 117 (2007).
- [75] A. Kievsky *et al.*, *J. Phys. G* **35**, 063101 (2008).
- [76] R. Schiavilla, private communications.
- [77] A. Baroni, L. Girlanda, A. Kievsky, L. E. Marcucci, R. Schiavilla, and M. Viviani, *Phys. Rev. C* **94**, 024003 (2016); Erratum: *Phys. Rev. C* **95**, 059902 (2017).
- [78] H. Krebs, E. Epelbaum, and U.-G. Meissner, *Ann. Phys.* **378**, 317 (2017).
- [79] L. E. Marcucci, R. Schiavilla, and M. Viviani, *Phys. Rev. Lett.* **110**, 192503 (2013).
- [80] I. Tews, T. Krüger, K. Hebeler, and A. Schwenk, *Phys. Rev. Lett.* **110**, 032504 (2013).
- [81] K. Hebeler, H. Krebs, E. Epelbaum, J. Golak and R. Skibinski, *Phys. Rev. C* **91**, 044001 (2015).
- [82] H. Krebs, A. Gasparyan, and E. Epelbaum, *Phys. Rev. C* **85**, 054006 (2012).
- [83] V. Bernard, E. Epelbaum, H. Krebs, and Ulf-G. Meißner, *Phys. Rev. C* **77**, 064004 (2008).

- [84] J.-I. Fujita and H. Miyazawa, *Prog. Theor. Phys.* **17**, 360 (1957).
- [85] A similar investigation has been conducted in Ref. [68],

where a different philosophy for the adjustment of the 3NF is pursued and a complete N^3LO 3NF is applied.